Letter

Intermittency of turbulent velocity and scalar fields using three-dimensional local averaging

Dhawal Buaria [1,2,*] and Katepalli R. Sreenivasan [1,3]

[1] *Tandon School of Engineering, New York University, New York, New York 11201, USA*

[2] *Max Planck Institute for Dynamics and Self-Organization, 37077 Göttingen, Germany*

[3] *Department of Physics and the Courant Institute of Mathematical Sciences, New York University, New York, New York 10012, USA*

(Received 17 April 2022; accepted 21 June 2022; published 8 July 2022)

An efficient approach for extracting three-dimensional local averages in spherical subdomains is proposed and applied to study the intermittency of small-scale velocity and scalar fields in direct numerical simulations of isotropic turbulence. We focus on the inertial-range scaling exponents of locally averaged energy dissipation rate, enstrophy, and scalar dissipation rate corresponding to the mixing of a passive scalar θ in the presence of a uniform mean gradient. The Taylor-scale Reynolds number R_λ goes up to 1300, and the Schmidt number Sc up to 512 (albeit at smaller R_λ). The intermittency exponent of the energy dissipation rate is $\mu \approx 0.23 \pm 0.02$, whereas that of enstrophy is slightly larger; trends with R_λ suggest that this will be the case even at extremely large R_λ. The intermittency exponent of the scalar dissipation rate is $\mu_\theta \approx 0.35$ for $\mathrm{Sc} = 1$. These findings are in essential agreement with previously reported results in the literature. We additionally obtain results for high Schmidt numbers and show that μ_θ decreases monotonically with Sc, either as $1/\log \mathrm{Sc}$ or a weak power law, suggesting that $\mu_\theta \to 0$ as $\mathrm{Sc} \to \infty$, reaffirming recent results on the breakdown of scalar dissipation anomaly in this limit.

DOI: 10.1103/PhysRevFluids.7.L072601

I. INTRODUCTION

A key characteristic of fully developed fluid turbulence is small-scale intermittency, referring to the sporadic generation of intense fluctuations of velocity gradients or velocity increments, which result in strong deviations from Gaussianity and necessitate anomalous corrections to the seminal mean-field description by Kolmogorov (1941) [1,2]. Given its practical importance in numerous physical processes [3–8], and its fundamental connection to the energy cascade [9], a quantitative characterization of intermittency is at the heart of turbulence theory [1,2] and modeling [10]. A key concept in understanding intermittency is the introduction of local averaging which allows a quantification of anomalous corrections to the mean-field description in some pertinent manner [11,12]. In general, for a fluctuating quantity $A(\mathbf{x}, t)$, its local average $A_r(\mathbf{x}, t)$ over a scale r can be defined as

$$A_r(\mathbf{x}, t) = \frac{3}{4\pi r^3} \int_{|\mathbf{x}'| \leqslant r} A(\mathbf{x} + \mathbf{x}', t)\, d\mathbf{x}'. \tag{1}$$

* dhawal.buaria@nyu.edu

Evidently, local averages are defined over a spherical volume to ensure isotropy with respect to the averaging scale size. However, such an averaging has not been possible until now because the full three-dimensional (3D) field is rarely available in experiments. So they have predominantly relied on surrogates, which are usually in the form of averages along a line or in a plane [2]. These methods are sometimes known to give different results compared to 3D local averages [13–16]. Even when the full 3D field is available in experiments, the data are restricted to low Reynolds numbers [17], where a plausible inertial range is not available. In contrast, direct numerical simulations (DNS) provide access to full 3D field at sufficiently large Reynolds numbers, but accurate spherical averaging needs some extra work, since the data are available on a Cartesian grid. Consequently, recent works have relied on 3D averages over cubical domains [16,18] which, while convenient, could retain some anisotropies.

In this work, we present a simple approach to efficiently and accurately obtain 3D local averages in spherical domains from the DNS data and apply it to study the intermittency of velocity and scalar fields. For the velocity field, we revisit inertial-range scaling of locally averaged energy dissipation rate and enstrophy [18,19]. For the scalar field, we consider the scaling of locally averaged scalar dissipation rate, and compare it to that of the energy dissipation rate. A key novelty is that we focus on mixing of low-diffusivity scalars (or high Schmidt numbers), which are notoriously difficult to obtain due to additional resolution constraints, and have been available only very recently at sufficiently high Reynolds numbers [20,21].

Our work confirms the past results obtained primarily in experiments using one or two-dimensional surrogates. Some important trends with Reynolds numbers are also highlighted. We also show that the intermittent character of the scalar dissipation disappears at high Schmidt numbers, consistent with Refs. [20,21].

II. BACKGROUND

The energy dissipation rate ϵ and the enstrophy Ω, defined, respectively, as

$$\epsilon = 2\nu S_{ij} S_{ij}, \quad \Omega = \omega_i \omega_i, \tag{2}$$

capturing the local straining and rotational motions, are central to our understanding of the small-scale structure of turbulence [22–26]. Here, ν is the kinematic viscosity, S_{ij} is the strain-rate tensor, and ω_i is the vorticity (and repeated indices imply summation). At high Reynolds numbers, these quantities become highly intermittent, so a means to characterizing them, following Kolmogorov (1962) [11], is to average them locally over a scale r and study these averages for a wide range of r. In particular, it is postulated that for the locally averaged energy dissipation ϵ_r, its second moment will scale as

$$\langle \epsilon_r^2 \rangle \sim r^{-\mu}, \tag{3}$$

for r in the inertial range, where the constant μ is termed as the "intermittency exponent." Note, other definitions of intermittency exponent are also possible, but they are mostly equivalent and give essentially the same value [27]; also see Sec. IV A. Based on theoretical grounds [23], a similar result is also anticipated for the locally averaged enstrophy Ω_r, with the same numerical value of the intermittency exponent. However, previous DNS data have suggested a slightly larger intermittency exponent for enstrophy [18,19].

The pertinent small-scale quantity when considering turbulent mixing of a passive scalar $\theta(\mathbf{x}, t)$ is the scalar dissipation rate

$$\chi = 2D|\nabla\theta|^2, \tag{4}$$

where D is the scalar diffusivity. It is well established that the scalar gradients and scalar increments also exhibit intermittency [2], and so, similar to ϵ_r and Ω_r, we can consider the scaling of χ_r [28]. The mixing process is controlled additionally by the Schmidt number $\mathrm{Sc} = \nu/D$. Obtaining data at

high Sc, while also keeping the Reynolds numbers acceptably high, is extremely challenging due to additional resolution constraints, and has only been possible very recently [20,21].

III. NUMERICAL APPROACH

A. Direct numerical simulations and database

The velocity data examined in this work are obtained by solving the incompressible Navier-Stokes equations:

$$\partial \mathbf{u}/\partial t + \mathbf{u}\cdot\nabla\mathbf{u} = -\nabla P + \nu\nabla^2\mathbf{u} + \mathbf{f}, \tag{5}$$

where $\mathbf{u}$ is the divergence free velocity field ($\nabla\cdot\mathbf{u} = 0$), P is the kinematic pressure and $\mathbf{f}$ is the large-scale forcing term to maintain statistical stationarity. Both deterministic and stochastic forcing schemes have been used, essentially giving identical results for small-scale statistics. The DNS corresponds to the canonical setup of isotropic turbulence in a periodic domain [29], allowing the use of highly accurate Fourier pseudospectral methods, with aliasing errors controlled using a combination of grid-shifting and truncation [30]. The database for the present work corresponds to recent works [31–34], with the Taylor-scale Reynolds number R_λ in the range 140–1300. Convergence with respect to resolution and statistical sampling has also been thoroughly established in all these previous works.

The passive scalar is obtained by simultaneously solving the advection-diffusion equation in the presence of a uniform mean-gradient:

$$\partial\theta/\partial t + \mathbf{u}\cdot\nabla\theta = -\mathbf{u}\cdot\nabla\Theta + D\nabla^2\theta. \tag{6}$$

The uniform mean-gradient is set along the first Cartesian direction: $\nabla\Theta = (G, 0, 0)$, and provides the forcing needed to achieve statistical stationarity for the scalar [35]. The database for scalars utilized here is the same as in our recent papers [20,21], and corresponds to R_λ in the range 140–650, and Sc in the range 1–512. As noted in Ref. [20], the data were generated using conventional Fourier pseudospectral methods for Sc = 1, and a hybrid approach for higher Sc [36–38]. This approach consisted of solving for the velocity field using standard pseudospectral approach with spatial resolutions of the order of the Kolmogorov length scale η_K; solving for the scalar field included using compact finite differences on a finer grid, so as to resolve the Batchelor scale $\eta_B = \eta_K \mathrm{Sc}^{-1/2}$ [39].

B. Local averaging procedure

To implement the 3D local averaging efficiently, Eq. (1) is rewritten as

$$A_r(\mathbf{x}, t) = \int_{\mathbf{x}'} G(\mathbf{x}')A(\mathbf{x}+\mathbf{x}', t)\, d\mathbf{x}', \tag{7}$$

$$\text{where} \quad G(\mathbf{x}') = \begin{cases} 3/4\pi r^3 & \text{for } |\mathbf{x}'| \leqslant r, \\ 0 & \text{for } |\mathbf{x}'| > r, \end{cases} \tag{8}$$

satisfying $\int_{\mathbf{x}'} G(\mathbf{x}')d\mathbf{x}' = 1$, represents an isotropic box filter [40]. We have essentially rewritten the local averaging procedure as a convolution. Following recent works in refs. [41,42], it can be shown that this convolution can be efficiently computed in the Fourier-space for any chosen value of r, as

$$\hat{A}_r(\mathbf{k}, t) = f(kr)\hat{A}(\mathbf{k}, t), \quad \text{where} \quad f(kr) = \frac{3[\sin(kr) - kr\cos(kr)]}{(kr)^3}. \tag{9}$$

Here, $\hat{(\cdot)}$ denotes the Fourier transform, $\mathbf{k}$ is the wave vector, with $|\mathbf{k}| = k$, and $f(kr)$ is the transfer function corresponding to $G(\mathbf{r})$. Unlike in previous works [16,18], this local averaging is evaluated exactly in an isotropic spherical volume. It can also be easily shown that this isotropic box filter also satisfies the consistency condition: $\langle A_r\rangle = \langle A\rangle$.

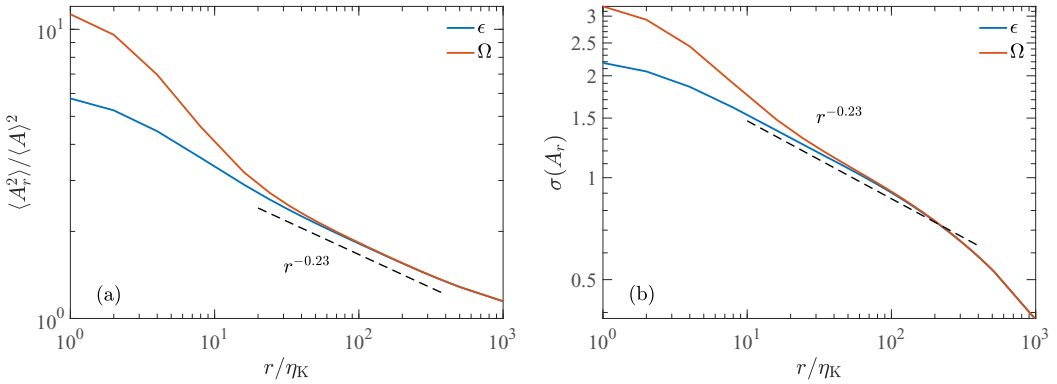

FIG. 1. (a) Second moment of locally averaged dissipation and enstrophy at $R_\lambda = 1300$. The intermittency exponent for dissipation is about $\mu = 0.23$ and that for enstrophy is slightly larger. (b) The variance of local averages as defined by Eq. (10).

IV. RESULTS

A. Energy dissipation rate and enstrophy

We first consider the intermittency of dissipation and enstrophy, a topic that has received considerable attention in the literature [18,19,22,25,43]. Figure 1(a) shows the second moments of locally averaged dissipation and enstrophy at $R_\lambda = 1300$ (the highest in the current work). As anticipated, for small r, the moments of local averages simply tend to those of instantaneous quantities, those for enstrophy being larger (as is known); whereas at large r, the moments tend to the same value of unity (as they should). In the inertial range, dissipation exhibits the power-law $r^{-0.23}$ (with an error bar of 0.02) for a reasonable range of r, implying $\mu \approx 0.23 \pm 0.02$, in very good agreement with previous works [27]. At the same time, within the same range of r, the enstrophy curve suggests a slightly larger intermittency exponent, consistent with previous works [18,19]; see later for more details.

An alternative means of extracting the intermittency exponent is to consider the variance of ϵ_r (and Ω_r), computed after subtracting the respective means for each r; for instance,

$$\sigma(\epsilon_r) = \langle(\epsilon_r - \langle\epsilon_r\rangle)^2\rangle/\langle\epsilon_r\rangle^2 = \langle\epsilon_r^2\rangle/\langle\epsilon\rangle^2 - 1; \tag{10}$$

note that $\langle\epsilon_r\rangle = \langle\epsilon\rangle$. The expectation is that $\sigma(\epsilon_r) \sim r^{-\mu}$ in the inertial range [27]. Figure 1(b) shows the variance of ϵ_r and Ω_r, and indeed the nature of their scaling follow expectations—although the scaling ranges are somewhat different from Fig. 1(a).

B. Effect of Reynolds number

To be stringent about the power law exponents, it is helpful to take the log-log derivatives (or the local slope) of the curves in Fig. 1(a). Figure 2(a) shows the local slope of second moments of ϵ_r and Ω_r for various R_λ. It can be seen that the quality of results in the inertial range depend on R_λ and, in fact, a constant local slope (corresponding to a true power-law) is clear only at the highest $R_\lambda = 1300$. However, guided by this feature, one can look for signs of approximate power laws at lower R_λ, and find slightly large exponent values.

It is worth noting that in Fig. 2(a), the local slope of enstrophy (in the inertial range) is always larger than that of dissipation for every R_λ. To better document this behavior, Fig. 2(b) shows the ratio of the local slope of enstrophy with respect to that of dissipation (in the spirit of extended self-similarity). Remarkably, the curves are always above unity in the inertial range. Further, there is a weak but clear tendency for this ratio to approach unity with increasing R_λ, but the rate of

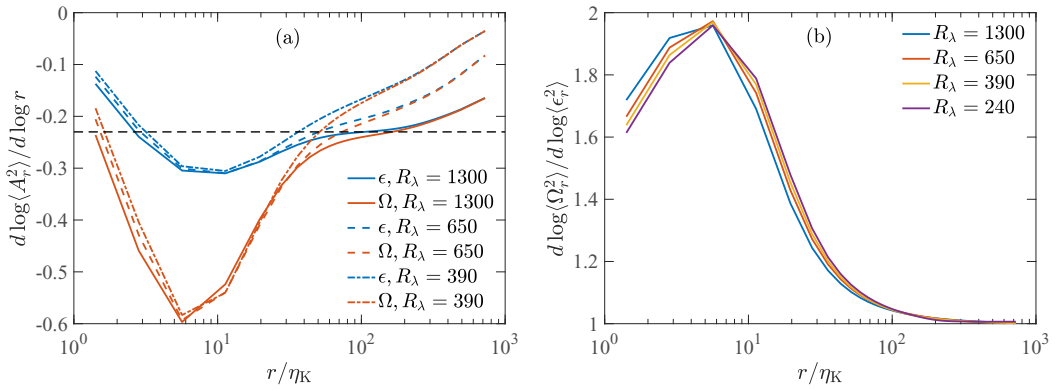

FIG. 2. (a) Local slopes of the second moment of locally averaged dissipation and enstrophy at different Reynolds numbers. The constancy of slopes improves as the inertial range enlarges with increasing Reynolds numbers. (b) Ratio of the two local slopes as a function of r. It is evident that the intermittency exponent for enstrophy is slightly larger and the approach towards unity as Reynolds number increases is extremely slow. Log denotes natural logarithm.

approach is so slow that the difference remains in place at all finite Reynolds numbers of interest. That is, enstrophy in the inertial range is slightly more intermittent than dissipation.

C. Scalar dissipation rate

We first consider locally averaged scalar dissipation rate for $\mathrm{Sc} = 1$. Figure 3(a) shows the second moments of locally averaged energy dissipation, enstrophy and scalar dissipation (at $R_\lambda = 650$), with the corresponding local slopes shown in Fig. 3(b). The intermittency exponent of the scalar μ_θ is larger than those of both dissipation and enstrophy, reaffirming past results that scalar gradients (at $\mathrm{Sc} = 1$) are more intermittent than velocity gradients [6]. While a clear plateau for dissipation and enstrophy is not achieved at $R_\lambda = 650$ [in Fig. 3(b)] the curve for scalar dissipation shows a very convincing plateau, giving $\mu_\theta \approx 0.35$. This result is in excellent agreement with earlier experimental results of Refs. [14,28].

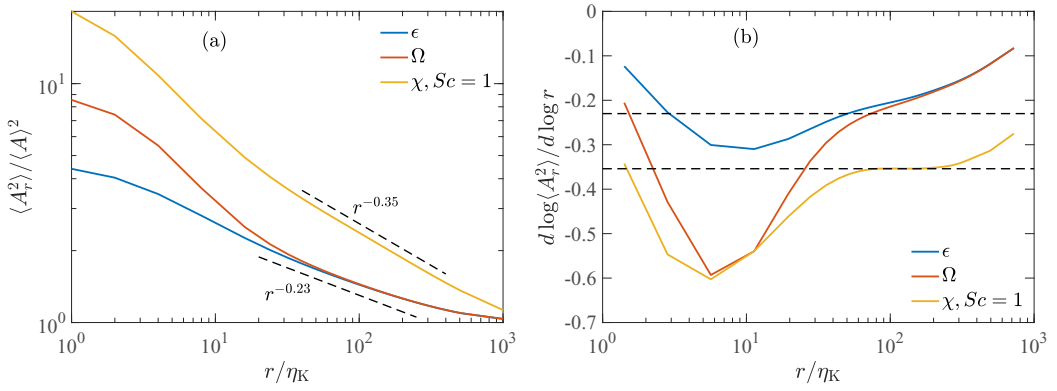

FIG. 3. (a) Second moment of locally averaged energy dissipation, enstrophy and scalar dissipation at $R_\lambda = 650$, with scalar at $\mathrm{Sc} = 1$. The intermittency exponent of scalar $\mu = 0.35$ is significantly larger. (b) The local slopes of quantities shown in panel (a) demonstrates that the inertial range scaling for the scalar is very robust. Log denotes natural logarithm.

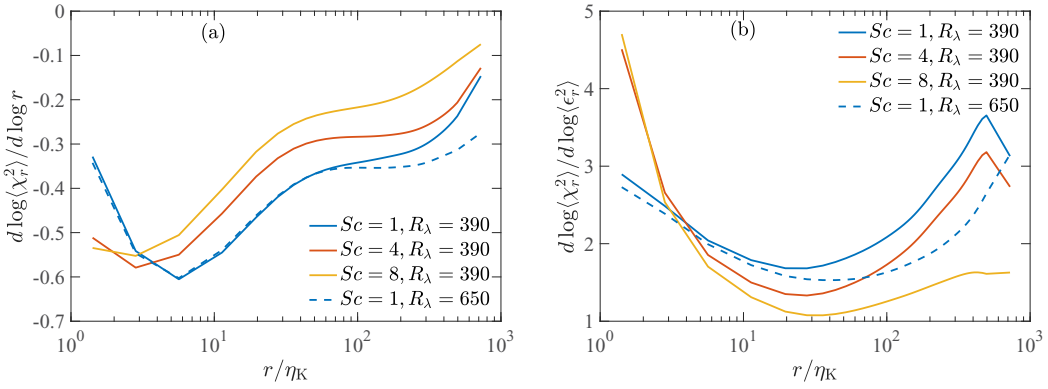

FIG. 4. (a) Local slopes of the second moment of locally averaged scalar dissipation at $R_\lambda = 390$ for Sc $=$ 1, 4, 8 and at $R_\lambda = 650$ for Sc $= 1$. (b) The ratio of the local slope of scalar dissipation to that of energy dissipation for same cases as shown in panel (a). Log denotes natural logarithm.

The effect of increasing Sc is considered next. Since increasing Sc imposes a stricter constraint on small-scale resolution, we consider data at slightly lower $R_\lambda = 390$, but still large enough to display inertial range characteristics. Figure 4(a) shows the local slope of second moment of scalar dissipation at $R_\lambda = 390$ and Sc $=$ 1–8. The curve corresponding to $R_\lambda = 650$ and Sc $= 1$ is also shown for comparison. The scalar intermittency exponent monotonically decreases with increasing Sc (also displaying a weak R_λ dependence).

Because of this possible R_λ-dependence, it is difficult to extract precisely the intermittency exponents at higher Sc. Instead, if we were to compare the ratio of μ_θ to μ, then a trend can be established; this should shed light on the asymptotic limit of Sc $\to \infty$. To this end, Fig. 4(b) shows the local slope of scalar dissipation with respect to that of energy dissipation. The R_λ-dependence is somewhat more prominent than in Fig. 4(a), likely because μ_θ seemingly has a stronger R_λ-dependence than μ. Nevertheless, it is evident that the ratio μ_θ/μ monotonically decreases with Sc.

For a definitive answer on the high Sc limit, one obviously needs to obtain data at substantially higher Sc at $R_\lambda = 390$ (and also at higher R_λ). But these are unlikely to be attained anytime soon. Instead, we analyze data at lower $R_\lambda = 140$, for which inertial range characteristics just begin to manifest [16,29]. Figure 5(a) shows the local slope of second moment of scalar dissipation with respect to that of energy dissipation up to Sc as high as 512. The curve corresponding to $R_\lambda = 390$ and Sc $= 8$ is also shown for comparison.

Two main conclusions can be drawn from this figure. First, the effect of R_λ is weaker at higher Sc [in comparison to that at Sc $= 1$, as evident from Fig. 4(b)]. Second, the ratio μ_θ/μ keeps decreasing further, possibly suggesting that $\mu_\theta \to 0$ as Sc $\to \infty$. We extract the ratio μ_θ/μ from Fig. 5(a) and plot its inverse as a function of Sc in Fig. 5(b). The data show a weak power-law dependence (with an exponent of about 0.16), though a log Sc-behavior is equally appropriate. The log Sc-behavior of μ/μ_θ is loosely based on how the mean scalar dissipation rate scales with Sc [21]. From a physical viewpoint, the result that $\mu_\theta \to 0$ implies that the locally averaged scalar dissipation rate becomes homogeneous and independent of r in the limit Sc $\to \infty$. This inference is consistent with recent results which demonstrate a lack of scalar dissipation anomaly as Sc $\to \infty$ (or $D \to 0$) [21].

V. CONCLUSIONS

In this work, we have performed local averaging of turbulent intermittent variables as they should be done: spherical averaging of three-dimensional quantities without using surrogates from one- or two-dimensional cuts, without the use of Taylor's frozen-flow hypothesis, or relying on cubical

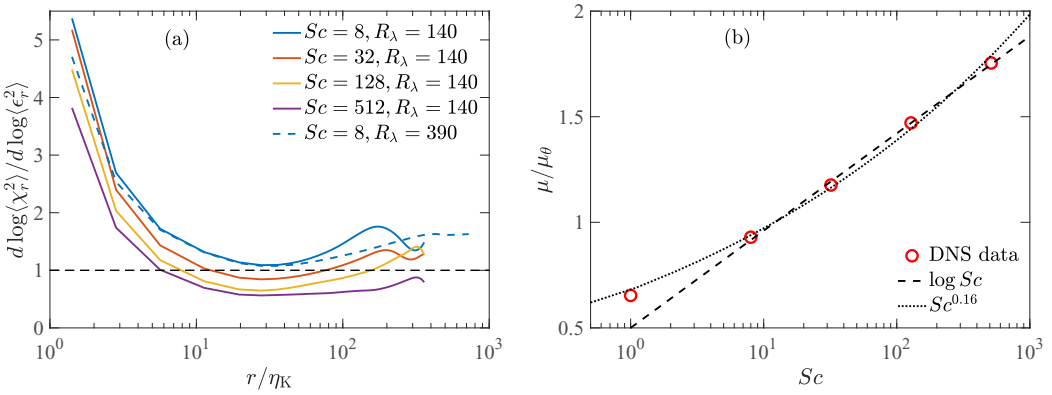

FIG. 5. (a) Ratio of local slopes of the second moments of locally averaged scalar dissipation and energy dissipation at $R_\lambda = 140$ for Sc $= 8, 32, 128, 512$ and at $R_\lambda = 390$ for Sc $= 8$. (b) Inverse of the inertial range exponents extracted from (a) as a function of Sc. Both power-law and log fits are shown. Log denotes natural logarithm.

subdomains. For the energy dissipation and enstrophy, we mostly recover past results with greater assurance; we feel more confident than ever that intermittency exponents do exist. Our results additionally suggest that enstrophy will always remain somewhat more intermittent than energy dissipation even at extremely large R_λ, reaffirming recent results of Ref. [26].

For the scalar dissipation, no previous studies existed on its scaling at high Schmidt numbers with large enough Reynolds number to obtain inertial range characteristics. In our simulations, the maximum allowable computational capacity has necessitated decreasing Sc with increasing R_λ. For Sc $= 1$, we were able to maintain R_λ as high as 650, whereas $R_\lambda = 140$ for the highest Sc $= 512$. It is unlikely that one can get much higher R_λ for such high Sc anytime soon. For these conditions, we have been able to extract the intermittency exponent for the scalar dissipation. For Sc $= 1$, it is very close to what had been deduced from earlier measurements of the full scalar dissipation using Taylor's hypothesis [14], and some surrogate quantities in planar cuts [28]. An important result is that the intermittency exponent for the scalar dissipation decreases either as a weak power of Sc or logarithmically, apparently to zero in the limit Sc $\to \infty$. This decrease is consistent with our recent results [20,21] that turbulence loses its ability to effectively mix passive scalars with very low diffusivity.

ACKNOWLEDGMENTS

We thank P. K. Yeung for comments on the draft and sustained collaboration over the years. D.B. gratefully acknowledge the Gauss Centre for Supercomputing e.V. [44] for providing computing time on the supercomputers JUQUEEN and JUWELS at Jülich Supercomputing Centre, where the simulations utilized in this work were primarily performed. The high Schmidt number simulations at $R_\lambda = 140$ (Sc $\geqslant 8$) and $R_\lambda = 390$ (Sc $= 8$) were performed together with Matthew Clay and P. K. Yeung using resources of the Oak Ridge Leadership Computing Facility (OLCF), under 2017 and 2018 INCITE Awards.

[1] U. Frisch, *Turbulence: The Legacy of Kolmogorov* (Cambridge University Press, Cambridge, UK, 1995).
[2] K. S. Sreenivasan and R. A. Antonia, The phenomenology of small-scale turbulence, Annu. Rev. Fluid Mech. **29**, 435 (1997).

[3] D. K. Wilson, J. C. Wyngaard, and D. I. Havelock, The effect of turbulent intermittency on scattering into an acoustic shadow zone, J. Acoust. Soc. Am. **99**, 3393 (1996).
[4] G. Falkovich, A. Fouxon, and M. G. Stepanov, Acceleration of rain initiation by cloud turbulence, Nature (London) **419**, 151 (2002).
[5] R. A. Shaw, Particle-turbulence interactions in atmospheric clouds, Annu. Rev. Fluid Mech. **35**, 183 (2003).
[6] K. R. Sreenivasan, Possible effects of small-scale intermittency in turbulent reacting flows, Flow, Turbul. Combust. **72**, 115 (2004).
[7] P. E. Hamlington, A. Y. Poludnenko, and E. S. Oran, Interactions between turbulence and flames in premixed reacting flows, Phys. Fluids **23**, 125111 (2011).
[8] D. Buaria, B. L. Sawford, and P. K. Yeung, Characteristics of backward and forward two-particle relative dispersion in turbulence at different Reynolds numbers, Phys. Fluids **27**, 105101 (2015).
[9] A. Tsinober, *An Informal Conceptual Introduction to Turbulence* (Springer, Berlin, 2009).
[10] C. Meneveau, Lagrangian dynamics and models of the velocity gradient tensor in turbulent flows, Annu. Rev. Fluid Mech. **43**, 219 (2011).
[11] A. N. Kolmogorov, A refinement of previous hypotheses concerning the local structure of turbulence in a viscous incompressible fluid at high Reynolds number, J. Fluid Mech. **13**, 82 (1962).
[12] A. M. Oboukhov, Some specific features of atmospheric turbulence, J. Fluid Mech. **13**, 77 (1962).
[13] L.-P. Wang, S. Chen, J. G. Brasseur, and J. C. Wyngaard, Examination of hypotheses in the Kolmogorov refined turbulence theory through high-resolution simulations. Part 1. Velocity field, J. Fluid Mech. **309**, 113 (1996).
[14] K. R. Sreenivasan, R. A. Antonia, and H. Q. Danh, Log-normality of temperature dissipation in a turbulent boundary layer, Phys. Fluids **20**, 1238 (1977).
[15] G. Stolovitzky, P. Kailasnath, and K. R. Sreenivasan, Kolmogorov's Refined Similarity Hypotheses, Phys. Rev. Lett. **69**, 1178 (1992).
[16] K. P. Iyer, K. R. Sreenivasan, and P. K. Yeung, Refined similarity hypothesis using three-dimensional local averages, Phys. Rev. E **92**, 063024 (2015).
[17] J. M. Lawson, E. Bodenschatz, A. N. Knutsen, J. R. Dawson, and N. A. Worth, Direct assessment of Kolmogorov's first refined similarity hypothesis, Phys. Rev. Fluids **4**, 022601(R) (2019).
[18] P. K. Yeung and K. Ravikumar, Advancing understanding of turbulence through extreme-scale computation: Intermittency and simulations at large problem sizes, Phys. Rev. Fluids **5**, 110517 (2020).
[19] S. Chen, K. R. Sreenivasan, and M. Nelkin, Inertial Range Scalings of Dissipation and Enstrophy in Isotropic Turbulence, Phys. Rev. Lett. **79**, 1253 (1997).
[20] D. Buaria, M. P. Clay, K. R. Sreenivasan, and P. K. Yeung, Turbulence is an Ineffective Mixer When Schmidt Numbers are Large, Phys. Rev. Lett. **126**, 074501 (2021).
[21] D. Buaria, M. P. Clay, K. R. Sreenivasan, and P. K. Yeung, Small-Scale Isotropy and Ramp-Cliff Structures in Scalar Turbulence, Phys. Rev. Lett. **126**, 034504 (2021).
[22] E. D. Siggia, Numerical study of small-scale intermittency in three-dimensional turbulence, J. Fluid Mech. **107**, 375 (1981).
[23] M Nelkin, Enstrophy and dissipation must have the same exponents in the high reynolds number limit of fluid turbulence, Phys. Fluids **11**, 2202 (1999).
[24] B. W. Zeff, D. D. Lanterman, R. McAllister, R. Roy, E. H. Kostelich, and D. P. Lathrop, Measuring intense rotation and dissipation in turbulent flows, Nature (London) **421**, 146 (2003).
[25] D. Buaria, A. Pumir, E. Bodenschatz, and P. K. Yeung, Extreme velocity gradients in turbulent flows, New J. Phys. **21**, 043004 (2019).
[26] D. Buaria and A. Pumir, Vorticity-Strain Rate Dynamics and the Smallest Scales of Turbulence, Phys. Rev. Lett. **128**, 094501 (2022).
[27] K. R. Sreenivasan and P. Kailasnath, An update on the intermittency exponent in turbulence, Phys. Fluids A: Fluid Dynam. **5**, 512 (1993).
[28] R. R. Prasad, C. Meneveau, and K. R. Sreenivasan, Multifractal Nature of the Dissipation Field of Passive Scalars in Fully Turbulent Flows, Phys. Rev. Lett. **61**, 74 (1988).

[29] T. Ishihara, T. Gotoh, and Y. Kaneda, Study of high-Reynolds number isotropic turbulence by direct numerical simulations, Ann. Rev. Fluid Mech. **41**, 165 (2009).
[30] R. S. Rogallo, Numerical experiments in homogeneous turbulence, NASA Technical Memo **81315** (1981).
[31] D. Buaria and K. R. Sreenivasan, Dissipation range of the energy spectrum in high Reynolds number turbulence, Phys. Rev. Fluids **5**, 092601(R) (2020).
[32] D. Buaria, E. Bodenschatz, and A. Pumir, Vortex stretching and enstrophy production in high Reynolds number turbulence, Phys. Rev. Fluids **5**, 104602 (2020).
[33] D. Buaria, A. Pumir, and E. Bodenschatz, Generation of intense dissipation in high Reynolds number turbulence, Philos. Trans. R. Soc. A **380**, 20210088 (2022).
[34] D. Buaria and K. R. Sreenivasan, Scaling of Acceleration Statistics in High Reynolds Number Turbulence, Phys. Rev. Lett. **128**, 234502 (2022).
[35] M. R. Overholt and S. B. Pope, Direct numerical simulation of a passive scalar with imposed mean gradient in isotropic turbulence, Phys. Fluids **8**, 3128 (1996).
[36] M. P. Clay, D. Buaria, T. Gotoh, and P. K. Yeung, A dual communicator and dual grid-resolution algorithm for petascale simulations of turbulent mixing at high Schmidt number, Comput. Phys. Commun. **219**, 313 (2017).
[37] M. P. Clay, D. Buaria, P. K. Yeung, and T. Gotoh, GPU acceleration of a petascale application for turbulent mixing at high Schmidt number using OpenMP 4.5, Comput. Phys. Commun. **228**, 100 (2018).
[38] M. P. Clay, D. Buaria, and P. K. Yeung, Improving scalability and accelerating petascale turbulence simulation using OpenMP, in *Proceedings of OpenMP Conference* (Stony Brook University, New York, 2017).
[39] G. K. Batchelor, Small-scale variation of convected quantities like temperature in turbulent fluid. 1. General discussion and the case of small conductivity, J. Fluid Mech. **5**, 113 (1959).
[40] S. B. Pope, *Turbulent Flows* (Cambridge University Press, Cambridge, UK, 2000).
[41] D. Buaria, A. Pumir, and E. Bodenschatz, Self-attenuation of extreme events in Navier-Stokes turbulence, Nat. Commun. **11**, 5852 (2020).
[42] D. Buaria and A. Pumir, Nonlocal amplification of intense vorticity in turbulent flows, Phys. Rev. Research **3**, L042020 (2021).
[43] S. Grossmann, D. Lohse, and A. Reeh, Different intermittency for longitudinal and transversal turbulent fluctuations, Phys. Fluids **9**, 3817 (1997).
[44] www.gauss-centre.eu.